chemosensors

MDPI

Article

Low-Cost Particulate Matter and Gas Sensor Systems for Roadside Environmental Monitoring: Mechanistic and Predictive Insights from One-Year Urban Measurements

Dan-Marius Mustață [1], Ioana Ionel [1,*], Daniel Bisorca [2] and Venera-Stanca Nicolici [1]

[1] Faculty of Mechanical Engineering, Universitatea Politehnica Timisoara, 300006 Timisoara, Romania; dan.mustata@student.upt.ro (D.-M.M.); venera-stanca.morar@student.upt.ro (V.-S.N.)
[2] Faculty of Civil Engineering, Universitatea Politehnica Timisoara, 300006 Timisoara, Romania; daniel.bisorca@upt.ro
* Correspondence: ioana.ionel@upt.ro; Tel.: +40-723349337

Abstract

Roadside public transport stops represent localized air pollution hotspots where short-term exposure may differ substantially from levels reported by urban background monitoring. This study investigates the application of low-cost air quality sensors for long-term characterization of particulate matter and gaseous pollutants in a traffic-dominated urban microenvironment. The novelty of this work lies in the combined use of collocated low-cost sensors, energy-independent solar-powered deployment, height-resolved placement representative of different breathing zones, and integrated statistical and predictive analysis to resolve exposure-relevant pollutant dynamics at a single transport stop. Hourly concentrations of particulate matter (PM) PM_1, $PM_{2.5}$, PM_{10}, nitrogen dioxide (NO_2), and ozone (O_3) were measured over one year at a roadside transport stop adjacent to a four-lane urban road carrying approximately 30,000 vehicles per day. Measurements were obtained using two collocated low-cost sensor units based on optical particle sensing for particulate matter and electrochemical sensing for gases, together with concurrent meteorological observations. Strong agreement between the two particulate matter sensors supported the use of averaged concentrations. Mean $PM_{2.5}$ concentrations were substantially higher in winter (32.4 $\mu g/m^3$) than in summer (10.4 $\mu g/m^3$), indicating pronounced seasonal variability. PM_1 and $PM_{2.5}$ exhibited closely aligned temporal patterns, while PM_{10} showed greater variability. NO_2 displayed sharp diurnal peaks associated with traffic activity, whereas O_3 exhibited opposing seasonal and diurnal behavior and was negatively correlated with both $PM_{2.5}$ ($r = -0.32$) and NO_2 ($r = -0.29$). One-hour-ahead predictive models incorporating meteorological and temporal variables achieved coefficients of determination up to 0.84. The results demonstrate that energy-independent low-cost sensor systems can robustly capture temporal patterns, pollutant interactions, and short-term predictability in localized roadside environments relevant to exposure assessment.

Keywords: gas sensors; low-cost electrochemical sensors; air quality monitoring; sensor systems and applications; environmental sensing; traffic-related emissions; urban microenvironments; mechanism-oriented analysis

Check for updates

Received: 28 December 2025
Revised: 18 January 2026
Accepted: 2 February 2026
Published: 4 February 2026

Copyright: © 2026 by the authors. Licensee MDPI, Basel, Switzerland. This article is an open access article distributed under the terms and conditions of the Creative Commons Attribution (CC BY) license.

1. Introduction

Urban air pollution remains a major environmental and public health challenge worldwide [1], particularly in traffic-dominated environments where human exposure is often

elevated and highly variable. Road transport is a primary source of both particulate matter and gaseous pollutants, contributing to complex mixtures that vary over short spatial and temporal scales [2,3]. Public transport stops located adjacent to busy roads represent localized microenvironments where individuals may experience short-term exposure levels that are not adequately represented by urban background monitoring stations.

Particulate matter (PM) encompasses a broad range of particle sizes and sources [4]. Fine particles ($PM_{2.5}$ and PM_1) are largely associated with combustion processes, including vehicle exhaust and secondary aerosol formation [5], and are of particular concern due to their ability to penetrate deep into the respiratory tract and enter the bloodstream [6]. Exposure to fine particulate matter has been linked to cardiovascular and respiratory disease, systemic inflammation, impaired lung function, thyroid carcinoma and increased mortality [7,8]. Coarse particles (PM_{10}), while less likely to reach the alveolar region, contribute to upper respiratory symptoms [9] and are commonly associated with mechanically generated sources such as road dust resuspension, tire and brake wear [10], and vehicle-induced turbulence [11].

Traffic-related gaseous pollutants further exacerbate health risks. Nitrogen dioxide (NO_2), a marker of combustion emissions, has been associated with airway inflammation, increased susceptibility to respiratory infections, and asthma exacerbation, particularly in children and other vulnerable populations [12–14]. Ozone (O_3), a secondary pollutant formed through photochemical reactions involving nitrogen oxides and volatile organic compounds, is a strong oxidant that can impair lung function, trigger respiratory symptoms, and increase hospital admissions during high-concentration episodes [15,16]. Near roadways, the interaction between freshly emitted nitrogen oxides and ozone leads to distinct spatial and temporal patterns that differ from those observed at urban background locations [17].

Beyond direct health impacts, traffic-related air pollution also affects the broader environment. Particulate matter influences atmospheric visibility and radiative balance [18], contributes to cloud formation processes [19], and deposits onto soil and water surfaces [20]. Nitrogen oxides (NO_x) play a role in acidification and eutrophication [21], while ozone damages vegetation, reduces crop yields, and impairs ecosystem productivity [22,23]. These combined impacts highlight the importance of monitoring multiple pollutants simultaneously when assessing the environmental footprint of urban transportation systems [24].

Exposure to air pollution within cities is highly heterogeneous. Conventional regulatory monitoring networks are designed to capture long-term trends and compliance at the city scale, but they often fail to resolve fine-scale variability in transport-related microenvironments such as roadside public transport stops [25]. Low-cost sensor systems offer a practical means to address this gap by enabling localized, high-resolution monitoring of pollutant dynamics under real-world conditions [26].

Within this context, the present study examines one year of hourly measurements of PM_1, $PM_{2.5}$, PM_{10}, NO_2, and O_3 at a roadside public transport stop adjacent to a heavily trafficked urban road. By analyzing seasonal, diurnal, and short-term variability, as well as pollutant relationships and predictability, this work provides insight into traffic-related air pollution dynamics and exposure-relevant patterns in a representative urban microenvironment.

2. Materials and Methods

2.1. Study Site and Traffic Characteristics

Air quality measurements were conducted over a continuous one-year period from June 2024 to May 2025 at a roadside public transport stop located adjacent to a four-lane urban road in a residential area on the outskirts of Timișoara, Romania. The roadway serves

as one of the main gateways into the city from the A1 motorway and functions as a frequent discharge route for vehicles entering the urban area. In addition to commuter traffic, the road provides access to a nearby zone characterized by a high density of warehouses, logistics centers, and industrial facilities, which contributes to sustained vehicle transit throughout the day.

The monitoring location represents a transport-related urban microenvironment characterized by direct proximity to emission sources, strong spatial gradients, and pronounced short-term temporal variability. Such environments are known to exhibit pollutant dynamics that are often not adequately captured by fixed regulatory monitoring stations, which are typically designed to represent urban background or area-wide conditions rather than localized exposure hotspots [27].

Average daily traffic on the adjacent roadway is approximately 30,000 vehicles per day. The traffic fleet is dominated by passenger cars and light-duty vehicles, while heavy-duty trucks are restricted on this road segment and permitted only under special authorization. Consequently, the contribution of heavy-duty vehicles to overall traffic volume and emissions is limited, although periodic transit associated with logistics and industrial activity occurs. This traffic composition is representative of many urban arterial roads connecting residential and industrial zones to city centers and has important implications for the relative contributions of exhaust-related fine particles and gaseous pollutants compared with mechanically generated coarse particulate matter from road dust resuspension, tire wear, and brake abrasion [28].

2.2. Sensor Systems and Measured Parameters

Measurements were obtained using two collocated low-cost, mobile air quality sensors manufactured by Airly Sp. Z o.o. (Krakow, Poland) [29]. These sensor units are designed for continuous outdoor operation and are increasingly deployed in dense monitoring networks to provide high-spatial and -temporal-resolution data. Their low cost and compact design make them particularly suitable for localized environmental monitoring, enabling assessment of exposure conditions at specific microenvironments such as public transport stops, intersections, and street canyons.

Both sensor units measured particulate matter mass concentrations in three size fractions, PM_1, $PM_{2.5}$, and PM_{10}, reported at hourly resolution. Meteorological parameters were recorded concurrently and included air temperature (°C), relative humidity (%), atmospheric pressure (hPa), wind speed (km/h), and wind direction (°). One of the two sensor units additionally measured gaseous pollutants, specifically NO_2 and O_3, reported in $\mu g/m^3$. The low-cost sensors used in this study were factory-calibrated by the manufacturer and deployed as part of an established monitoring platform. While no additional site-specific calibration against FRM/FEM reference instruments was performed for gaseous pollutants, the study focuses on relative temporal variability, pollutant interactions, and short-term predictability rather than on absolute concentration equivalence with regulatory measurements.

Particulate matter concentrations were measured using optical particle sensing based on light-scattering principles. Optical particle sensors do not provide information on chemical composition; therefore, source apportionment between exhaust and non-exhaust emissions cannot be directly resolved and was not the objective of this study. Ambient air is actively drawn through a sensing chamber, where suspended particles intersect a focused light beam generated by a laser diode. Scattered light is detected by photodiodes, and particle size and number concentration are estimated based on scattering intensity and angular distribution. Mass concentrations of PM_1, $PM_{2.5}$, and PM_{10} are derived through size classification and manufacturer-specific calibration algorithms that account for particle

size distribution and optical properties. Optical particle counters are widely used in low-cost PM sensing and have been shown to provide reliable information on temporal variability and trends, particularly when sensors are deployed consistently and evaluated through collocated measurements [30,31].

Gaseous pollutants were measured using electrochemical sensing elements, a mature and widely applied technology in low-cost gas sensing. Electrochemical sensors generate an electrical signal proportional to the concentration of a target gas through redox reactions occurring at the sensing electrode. In the Airly units used in this study, electrochemical cells were employed for the detection of NO_2 and O_3. These sensors provide sufficient sensitivity at ambient concentration levels and are well suited for monitoring traffic-related gases under outdoor conditions. According to manufacturer specifications, the electrochemical gas sensors integrated in the Airly PM+GAS unit have a nominal operating range up to 4000 ppb with a resolution of 1 ppb. Expressed in mass concentration units consistent with this study, this corresponds to approximately 0–7520 $\mu g\ m^{-3}$ for NO_2 and 0–7840 $\mu g\ m^{-3}$ for O_3 under standard ambient conditions, with corresponding mass-concentration resolutions of approximately 1.9 $\mu g\ m^{-3}$ [29]. These ranges comfortably encompass the concentration levels encountered in urban background and traffic-influenced environments. As with other electrochemical sensors, their response may be influenced by temperature, humidity, and potential cross-sensitivities, which are addressed through concurrent meteorological measurements and internal compensation algorithms [32–34].

Data acquisition and logging were handled automatically by the Airly monitoring system. Sensor measurements were transmitted at regular intervals via the integrated communication module to the manufacturer's cloud-based data platform, where they were stored and made available for retrieval and analysis. No local data storage (e.g., memory card–based logging) was used at the monitoring site. Cloud-based storage ensured continuous data availability, redundancy, and protection against data loss during long-term outdoor deployment.

By integrating optical particulate sensing and electrochemical gas sensing within a single low-cost platform, the Airly sensor systems enable simultaneous monitoring of particulate and gaseous pollutants relevant to urban air quality and human exposure. While such sensors are not intended to replace reference-grade instrumentation for regulatory compliance, their ability to capture high-resolution temporal variability and relative concentration changes makes them particularly valuable for application-driven studies focused on localized environments, source influences, and exposure dynamics.

Short-term predictive models, shown in the Results Section, were trained using the full set of valid hourly observations collected over the one-year monitoring period. The training dataset included pollutant concentrations ($PM_{2.5}$, NO_2, and O_3), concurrent meteorological variables (air temperature, relative humidity, atmospheric pressure, wind speed, and wind direction), and temporal indicators (hour of day, day of week). Autoregressive terms, consisting of pollutant concentrations from preceding hours, were included to capture short-term persistence. Model training and evaluation were performed using temporally ordered data to preserve the chronological structure of the time series.

2.3. Sensor Placement and Transport Stop Configuration

The monitoring site was located within a public transport stop enclosure, located 1.0 m away from the side of the road, consisting of three vertical walls and a roof, with the front side fully open and directly facing the adjacent roadway. This semi-enclosed geometry allows direct inflow of traffic-related pollutants into the stop area while partially limiting lateral ventilation. As a result, the enclosure forms a localized exposure microenvironment

representative of conditions experienced by passengers waiting inside the stop, rather than open-road conditions alone.

The two air quality sensor units were installed at different heights within the enclosure to reflect exposure conditions relevant to distinct population groups. The sensor measuring both particulate matter and gaseous pollutants (model: Airly Aura PM & Gas Sensor [29], production year 2021) was mounted at approximately 1.0 m above ground level, representing a typical breathing height for young children, while the particulate matter sensor (model: Airly Pure [29], production year 2020) was installed at approximately 1.7 m, corresponding to a representative adult breathing height. According to manufacturer specifications, the sensing components of the sensors and performance characteristics are equivalent, which is supported by the strong cross-sensor agreement observed in the data, even though produced across two different years.

Both sensors were positioned in close proximity to the roadway-facing opening of the enclosure to ensure direct exposure to traffic emissions while maintaining consistent enclosure effects.

The entire monitoring installation was mounted on a mobile platform equipped with wheels, allowing flexible deployment and relocation without modification to existing infrastructure.

A photograph of the mobile, solar-powered air quality monitoring system deployed at the roadside public transport stop is shown in Figure 1, illustrating the semi-enclosed stop geometry, proximity to traffic lanes, and real-world installation conditions.



Figure 1. Photograph of the mobile air quality monitoring system at the roadside public transport stop.

This mobile configuration supports application-driven monitoring in locations where permanent installations or grid power access may be limited.

2.4. Power Supply and Electronic System

The air quality sensors were integrated into a custom-built autonomous power supply system designed for continuous outdoor operation. The system combines photovoltaic energy harvesting, battery storage, and regulated power delivery to ensure stable sensor operation independent of grid power.

Electrical power is provided by a photovoltaic array consisting of four 50 W solar panels connected to a solar charge controller (12/24 V, 30 A). The charge controller regulates battery charging and provides protection against overcharge and deep discharge. Energy storage is provided by a 12 V, 110 Ah battery, which directly supplies power to the sensing units and buffers short-term fluctuations in solar input, ensuring uninterrupted operation. Dedicated fuses are installed on individual power branches to provide electrical protection and fault isolation.

An inverter (12 V to 230 V AC, 250 W) and an auxiliary grid-powered charger (12 V, 15 A) are included to allow backup charging during extended periods of low solar irradiance. Under normal operating conditions, however, the system operates exclusively on solar energy. Both Airly sensor units are powered from the regulated 12 V DC output, minimizing conversion losses and electrical noise.

This solar-powered electronic system enables sustainable, autonomous deployment of low-cost air quality sensors at locations where permanent grid access is impractical, supporting long-term, high-resolution environmental monitoring.

2.5. Time Handling and Data Quality Control

All timestamps were interpreted as local Europe/Bucharest time, with appropriate handling of daylight-saving time transitions. Data quality control procedures included assessment of data completeness, identification of missing or anomalous values, and evaluation of temporal continuity. Data availability exceeded 99% across the monitoring period.

Cross-sensor agreement for particulate matter measurements was evaluated using paired hourly observations from the two collocated sensors. Strong agreement was observed across all particulate size fractions, indicating consistent long-term performance under outdoor conditions. Given this high level of agreement, the arithmetic mean of the two particulate matter sensors was used as the best-estimate PM time series for all subsequent analyses. This approach reduces sensor-specific noise while preserving true temporal variability and is consistent with established practices for collocated low-cost sensor deployments.

Precipitation periods were not explicitly excluded; however, given the long-term scope of the analysis, precipitation-related effects are expected to contribute primarily to short-term variability rather than to the systematic temporal patterns discussed here. Precipitation-related effects are expected to contribute primarily to episodic short-term variability.

Signal filtering, temperature and humidity compensation for the electrochemical sensors, and low-level data preprocessing are implemented within the manufacturer's platform and are not publicly disclosed. The present analysis was based on quality-controlled hourly outputs provided by the system, with additional averaging and validation steps described herein.

2.6. Inter-Comparison with Gravimetric Reference Measurements for PM2.5 and PM10

To evaluate potential systematic bias in the optical particulate matter measurements, including possible temperature-dependent effects, an inter-comparison was conducted between the Airly sensors and gravimetric reference measurements during two contrasting seasonal periods. Gravimetric $PM_{2.5}$ and PM_{10} measurements were performed over seven consecutive 24 h sampling periods during winter (27 December 2024–2 January 2025) and summer (1–7 June 2024). Gravimetric sampling was conducted using a filter-based impactor method with daily sampling intervals from 00:00 to 00:00 local time. The gravimetric impactors used for $PM_{2.5}$ and PM_{10} measurements are metrologically certified and routinely

calibrated as part of the authors' laboratory instrumentation, which operates under an ISO/IEC 17025:2017 [35] accredited quality management system.

Hourly Airly PM measurements from both collocated sensors were aggregated to 24 h means over identical 00:00–00:00 intervals to ensure temporal alignment with the gravimetric samples. Daily averages were first computed independently for each sensor, after which the arithmetic mean of the two sensors was used as the best-estimate Airly concentration. Prior to comparison with gravimetric data, cross-sensor consistency was evaluated for each period to confirm stable and coherent sensor behavior.

Agreement between Airly and gravimetric measurements was assessed using paired daily differences (Airly − gravimetric). For each PM fraction and season, mean bias was calculated together with 95% confidence intervals using Student's t distribution (degrees of freedom = 6). Additional performance metrics included root mean square error (RMSE) and mean absolute error (MAE). This inter-comparison was intended to quantify uncertainty and assess agreement under real-world operating conditions rather than to establish regulatory equivalence.

3. Results

To facilitate interpretation of long-term pollutant behavior and reduce short-term variability associated with hourly fluctuations, seven-day rolling mean concentrations were calculated for $PM_{2.5}$, NO_2, and O_3. This temporal smoothing emphasizes seasonal and sustained trends while preserving continuity across the full monitoring period. The resulting time series reveals clear contrasts in the temporal behavior of particulate matter and gaseous pollutants over the one-year deployment. Elevated $PM_{2.5}$ concentrations are evident during winter months, with substantially lower levels during summer, whereas ozone displays an opposing seasonal cycle characterized by higher concentrations in spring and summer. Nitrogen dioxide exhibits pronounced variability throughout the year, with episodic increases superimposed on broader seasonal patterns. These long-term trends, illustrated in Figure 2, provide an overview of pollutant dynamics and establish the context for the detailed statistical, seasonal, and diurnal analyses presented in the following sections.

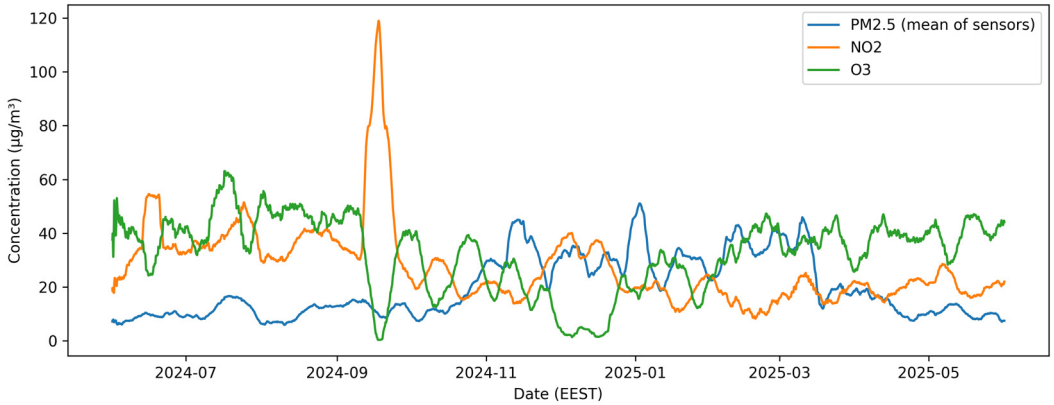


Figure 2. Seven-day rolling mean time series of $PM_{2.5}$ (mean of two sensors), NO_2, and O_3 ($\mu g/m^3$).

To provide regulatory context for the observed concentrations, measured pollutant levels were evaluated relative to applicable European Union and Romanian air quality standards established under European Directive 2008/50/EC and Romanian Law 104 15.06.2011 [36,37]. For fine particulate matter, the EU annual mean limit value for $PM_{2.5}$ is 25 $\mu g/m^3$, while NO_2 is regulated through an annual mean limit of 40 $\mu g/m^3$ and an hourly mean limit of 200 $\mu g/m^3$, not to be exceeded more than 18 times per year.

O_3 is subject to a target value defined as a maximum daily 8-h mean concentration of 120 μg/m^3. These reference values are used in the present study solely to contextualize the magnitude of observed concentrations and facilitate comparison with established air quality benchmarks, rather than to assess regulatory compliance at the monitoring site.

3.1. Data Coverage and Sensor Agreement

The final dataset comprised 8762 hourly observations, corresponding to a complete annual cycle of measurements, with data availability exceeding 99% for all particulate matter size fractions (PM_1, $PM_{2.5}$, and PM_{10}) and gaseous pollutants (NO_2 and O_3). Data completeness was consistently high throughout the monitoring period, with only isolated gaps attributable to short communication interruptions or routine maintenance, and no extended periods of missing data. This high temporal coverage enabled robust characterization of diurnal, weekly, and seasonal variability.

Cross-verification of the two collocated particulate matter sensors demonstrated very strong agreement across all size fractions. Paired hourly concentrations of PM_1, $PM_{2.5}$, and PM_{10} exhibited close correspondence over the full range of observed values, with stable relationships maintained across seasons and traffic conditions. No systematic divergence between the two sensors was observed, indicating consistent sensor performance during long-term outdoor deployment. Short-term variability and peak events were captured synchronously by both instruments, further supporting the reliability of the measurements.

The resulting dataset provides a robust foundation for the temporal, statistical, and predictive analyses presented in the following sections.

3.2. Inter-Comparison with Gravimetric Reference Measurements

During both winter and summer inter-comparison periods, the two collocated Airly sensors exhibited very strong agreement. Pearson correlation coefficients exceeded 0.99 for both $PM_{2.5}$ and PM_{10} in each season, and mean daily differences between sensors were approximately 1 μg m^{-3} or less. This high level of consistency supports the use of averaged sensor values for subsequent analysis and indicates stable sensor performance under both cold and warm ambient conditions.

To assess agreement between the Airly optical sensors and a reference method, daily 24 h mean $PM_{2.5}$ and PM_{10} concentrations were compared against gravimetric measurements during two seven-day periods representing contrasting thermal conditions.

For the summer period (1–7 June 2024), mean daily $PM_{2.5}$ concentrations measured by the Airly sensors were substantially lower, typically between 5 and 11 μg m^{-3}. Comparison with gravimetric measurements yielded a mean $PM_{2.5}$ bias of +0.13 μg m^{-3}, with a 95% confidence interval of −0.14 to +0.39 μg m^{-3}, again indicating no statistically significant bias. For PM_{10}, the mean bias was +0.29 μg m^{-3} (95% CI: +0.04 to +0.54 μg m^{-3}). RMSE values were below 0.4 μg m^{-3} for both fractions, reflecting close agreement during warm-season conditions.

For the winter period (27 December 2024–2 January 2025), mean daily $PM_{2.5}$ concentrations measured by the Airly sensors ranged from approximately 33 to 77 μg m^{-3}. Relative to the gravimetric reference, the Airly sensors exhibited a mean $PM_{2.5}$ bias of +0.90 μg m^{-3}, with a 95% confidence interval of −0.35 to +2.16 μg m^{-3}. The confidence interval included zero, indicating no statistically significant bias at the 95% level. For PM_{10}, the mean bias was +0.56 μg m^{-3} (95% CI: +0.07 to +1.04 μg m^{-3}). Error magnitudes were modest, with RMSE values of 1.55 μg m^{-3} for $PM_{2.5}$ and 0.74 μg m^{-3} for PM_{10}.

Across both seasons, bias magnitudes remained small and positive for both $PM_{2.5}$ and PM_{10}. Importantly, no reversal in bias sign was observed between winter and sum-

mer, and no evidence of systematic underestimation of $PM_{2.5}$ during warm conditions or overestimation during cold conditions was identified.

3.3. Seasonal Descriptive Statistics

Seasonal distributions of $PM_{2.5}$, NO_2, and O_3 are summarized in Tables 1–3. Fine PM exhibited pronounced seasonal variability, with substantially higher concentrations during winter compared with other seasons. Mean $PM_{2.5}$ concentrations reached 32.4 μg/m^3 in winter, decreasing to 20.6 μg/m^3 in autumn, 15.7 μg/m^3 in spring, and 10.4 μg/m^3 in summer. Upper-percentile values followed a similar pattern, with the 90th percentile reaching 48.4 μg/m^3 in winter, indicating frequent elevated concentration episodes during this period. The observed seasonal contrasts in particulate matter concentrations primarily reflect differences in atmospheric dispersion conditions, with winter characterized by reduced boundary-layer height, more frequent thermal inversions, and lower wind speeds that favor pollutant accumulation, while summer conditions promote more efficient dilution through enhanced mixing.

Table 1. Seasonal distribution of $PM_{2.5}$ (μg/m^3).

Season	Mean	SD	Median	P90
Winter	32.40	14.38	30.93	48.36
Spring	15.71	13.36	12.51	29.41
Summer	10.40	5.21	9.80	17.04
Autumn	20.64	14.81	16.50	38.63

Table 2. Seasonal distribution of NO_2 (μg/m^3).

Season	Mean	SD	Median	P90
Winter	20.37	13.63	19.65	38.59
Spring	19.90	12.53	17.89	33.93
Summer	37.57	20.36	32.51	62.35
Autumn	32.52	31.60	25.46	57.43

Table 3. Seasonal distribution of O_3 (μg/m^3).

Season	Mean	SD	Median	P90
Winter	23.61	19.81	21.47	51.85
Spring	38.57	22.52	36.54	69.57
Summer	43.95	47.52	26.75	107.65
Autumn	24.04	22.29	20.92	51.63

NO_2 also showed seasonal variability, although with a different magnitude and pattern than particulate matter. Mean NO_2 concentrations ranged from 19.9 μg/m^3 in spring to 37.6 μg/m^3 in summer, with elevated upper-percentile values observed during summer and autumn. This indicates substantial short-term variability and the presence of episodic concentration peaks across multiple seasons.

In contrast, O_3 exhibited an opposing seasonal cycle. Mean O_3 concentrations were lowest during winter (23.6 μg/m^3) and autumn (24.0 μg/m^3) and increased markedly during spring (38.6 μg/m^3) and summer (44.0 μg/m^3). The highest variability and extreme values were observed in summer, with 90th percentile concentrations exceeding 100 μg/m^3, reflecting enhanced photochemical activity during warmer months.

In Figure 3, frequency denotes the number of hourly observations falling within each concentration bin, illustrating how often specific concentration ranges occurred over the monitoring period.

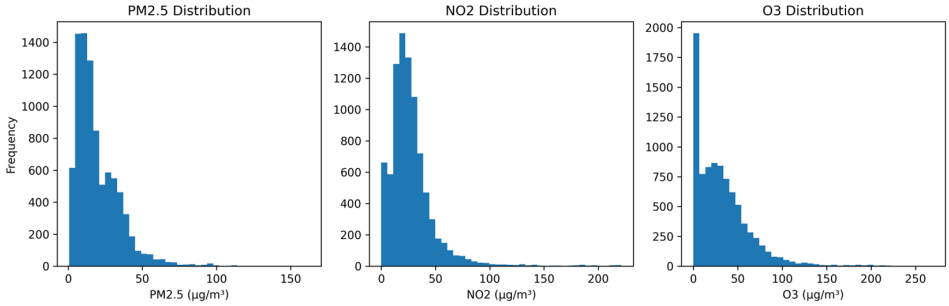


Figure 3. One-dimensional distributions of hourly $PM_{2.5}$, NO_2, and O_3 concentrations over the monitoring period.

3.4. Temporal Structure and Heat-Map Analysis

Heat-map representations of hourly concentrations by weekday and by month reveal pronounced and systematic diurnal and seasonal structure for all analyzed pollutants.

$PM_{2.5}$ concentrations exhibit clear weekday-dependent patterns, with distinct morning and evening peaks occurring during typical commuting hours and reduced concentrations during late night and early morning periods (Figures 4 and 5). These peaks are consistently more pronounced on weekdays compared with weekends, indicating strong temporal modulation linked to daily activity patterns. Seasonal heat maps further demonstrate that these diurnal peaks are amplified during winter and transitional seasons, while overall concentrations remain lower and more uniform during summer months.

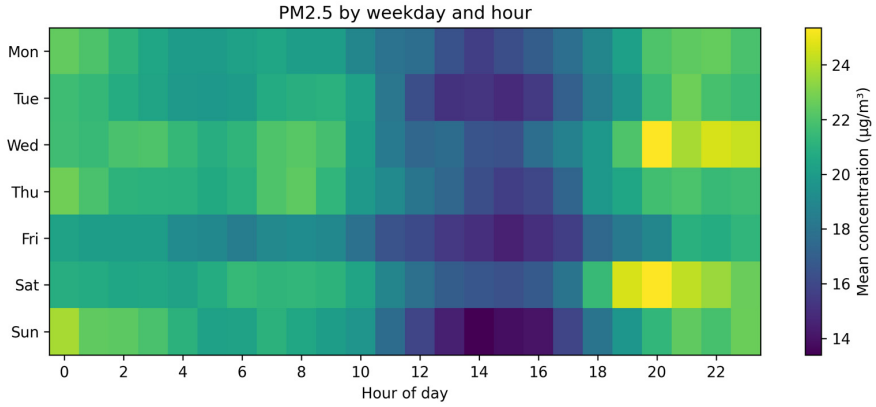


Figure 4. Heat map of mean $PM_{2.5}$ concentrations ($\mu g/m^3$) by weekday and hour of day.

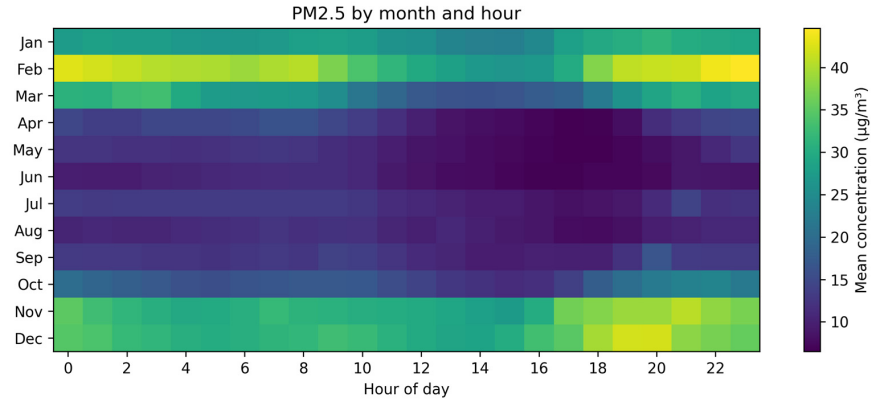


Figure 5. Heat map of mean $PM_{2.5}$ concentrations ($\mu g/m^3$) by month and hour of day.

NO_2 exhibits even sharper diurnal structure than $PM_{2.5}$, with narrow concentration maxima closely aligned with weekday morning and evening rush hours (Figures 6 and 7).

Weekend concentrations are substantially reduced across most hours of the day, and nighttime levels remain consistently low, highlighting strong short-term variability. Monthly heat-map analysis shows that elevated NO_2 concentrations persist across multiple seasons but with increased intensity during periods associated with high traffic activity.

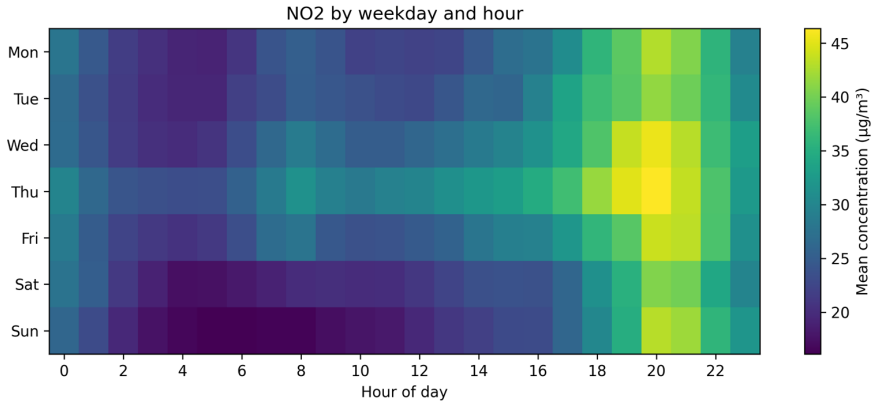


Figure 6. Heat map of mean NO_2 concentrations ($\mu g/m^3$) by weekday and hour of day.

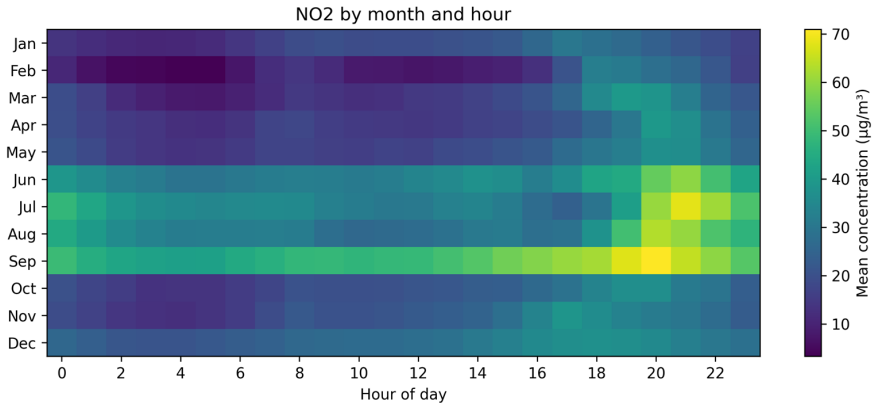


Figure 7. Heat map of mean NO_2 concentrations ($\mu g/m^3$) by month and hour of day.

In contrast, O_3 displays a distinctly different temporal structure (Figures 8 and 9). O_3 concentrations peak during midday hours and are highest during spring and summer months, with minimal differentiation between weekdays and weekends. Nighttime concentrations are consistently low across all seasons. This contrasting behavior highlights the different temporal regimes governing primary traffic-related pollutants and secondary photochemically formed ozone.

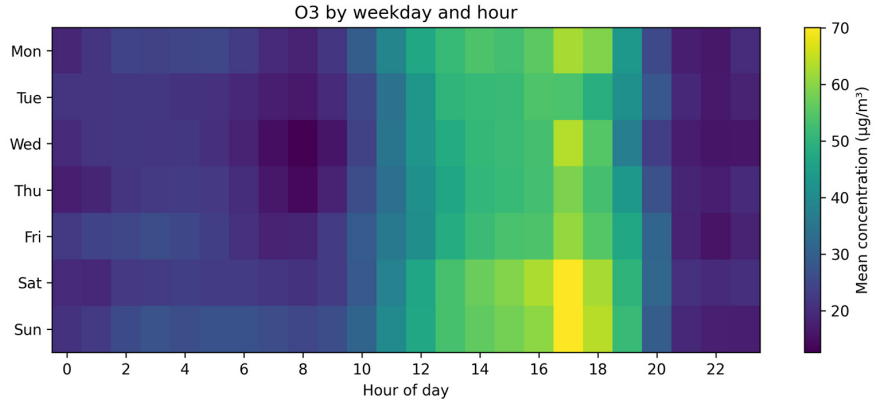


Figure 8. Heat map of mean O_3 concentrations ($\mu g/m^3$) by weekday and hour of day.

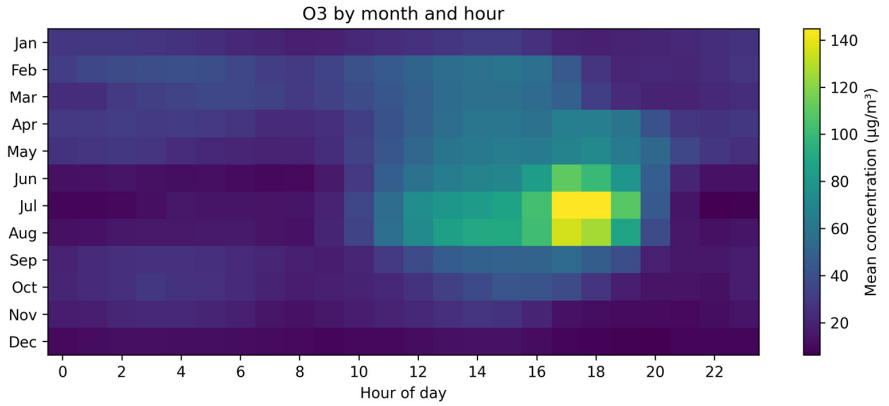


Figure 9. Heat map of mean O_3 concentrations ($\mu g/m^3$) by month and hour of day.

3.5. Pollutant Relationship

Table 4 summarizes the Pearson correlation coefficients between $PM_{2.5}$, NO_2, and O_3 based on the full hourly dataset. $PM_{2.5}$ and NO_2 exhibit a weak inverse correlation ($r = -0.12$), indicating limited linear association between fine particulate matter and nitrogen dioxide on an hourly basis despite their common traffic-related origin. This weak relationship reflects differing atmospheric lifetimes and responses to meteorological conditions.

Table 4. Pearson correlations between $PM_{2.5}$, NO_2, and O_3.

Pollutant Pair	Pearson r	Interpretation
$PM_{2.5}$–NO_2	−0.12	Weak inverse association
$PM_{2.5}$–O_3	−0.32	Moderate inverse association
NO_2–O_3	−0.29	Moderate inverse association

In contrast, O_3 shows moderate negative correlations with both $PM_{2.5}$ ($r = -0.32$) and NO_2 ($r = -0.29$). These inverse relationships are consistently observed across the dataset and indicate that elevated O_3 concentrations tend to coincide with lower levels of primary traffic-related pollutants. The magnitude of these correlations suggests a systematic but nonlinear interaction rather than direct coupling. Together, the correlation structure highlights distinct temporal and chemical regimes for primary pollutants and secondary ozone and provides a quantitative basis for the contrasting diurnal and seasonal patterns observed in the heat-map analyses.

3.6. Short-Term Predictive Modelling

Predictive models were developed to forecast one-hour-ahead pollutant concentrations using a combination of meteorological variables, temporal indicators, and autoregressive terms derived from the observed time series. Predictor variables included air temperature, relative humidity, atmospheric pressure, wind speed and direction, cyclic representations of hour of day, and recent concentration history through lagged terms. This formulation was applied consistently across pollutants to assess short-term predictability under real-world conditions.

Model performance is summarized in Table 5. For PM, predictive skill was high across all size fractions. The random forest model achieved coefficients of determination (R^2) of 0.84 for PM_1, 0.83 for $PM_{2.5}$, and 0.81 for PM_{10}, representing a clear improvement over a simple persistence baseline. Root mean square error (RMSE) values for the best-performing models were 2.1 $\mu g/m^3$ for PM_1, 2.8 $\mu g/m^3$ for $PM_{2.5}$, and 3.4 $\mu g/m^3$ for PM_{10}, indicating good agreement between predicted and observed concentrations.

Table 5. One-hour-ahead predictive model performance (R^2 and RMSE).

Target	Baseline R^2	Linear Model R^2	Random Forest R^2	RMSE (Best Model, μg/m^3)
PM_1	0.78	0.83	0.84	2.10
$PM_{2.5}$	0.81	0.84	0.83	2.80
PM_{10}	0.76	0.80	0.81	3.40
NO_2	0.69	0.75	0.78	5.00
O_3	0.62	0.70	0.73	6.80

For gaseous pollutants, predictive performance was more variable but remained substantial. One-hour-ahead forecasts achieved R^2 values of 0.78 for NO_2 and 0.73 for O_3, with RMSE values of approximately 5.0 μg/m^3 and 6.8 μg/m^3, respectively. Across all pollutants, models consistently outperformed the persistence baseline, demonstrating that short-term concentration variability contains systematic structure that can be captured using combined meteorological and temporal information.

4. Discussion

The combined descriptive, statistical, and predictive analyses consistently indicate a traffic-dominated pollution regime at the roadside public transport stop. Across all pollutants, short-term variability is primarily governed by emission timing and proximity to traffic, while longer-term seasonal contrasts are largely driven by changes in atmospheric dispersion rather than by variations in emission intensity. This separation of temporal scales provides a coherent framework for interpreting pollutant behavior in transport-related urban microenvironments.

Before interpreting these seasonal patterns mechanistically, it is important to consider potential instrumental contributions to the observed $PM_{2.5}$ contrasts.

The gravimetric inter-comparison results provide important context for interpreting the pronounced seasonal and diurnal $PM_{2.5}$ patterns observed in the long-term dataset. Optical particulate sensors are known to exhibit potential temperature-dependent behavior due to thermal effects on light sources and photodetectors. Such effects could, in principle, lead to apparent overestimation under cold conditions and underestimation under warm conditions if not adequately compensated.

However, the present inter-comparison does not support the presence of a strong temperature-dependent bias of this type. For $PM_{2.5}$, mean bias relative to gravimetric measurements was small and statistically indistinguishable from zero in both winter and summer. For PM_{10}, a small positive bias was observed in both seasons, but its magnitude (<1 μg m^{-3}) was negligible relative to ambient concentration levels and well within typical environmental variability. Crucially, no sign reversal in bias was observed between cold and warm periods, which would be expected if temperature-dependent optical effects dominated the measurements.

These findings indicate that while minor temperature-related sensor effects cannot be entirely excluded, they are unlikely to account for the large seasonal contrasts in $PM_{2.5}$ concentrations observed at the site. Instead, the elevated wintertime $PM_{2.5}$ levels are more plausibly explained by reduced atmospheric dispersion, frequent stable boundary layer conditions, and enhanced accumulation of fine particles during cold periods, rather than by instrumental artifacts. The close agreement between two independent sensors during both seasons further constrains the magnitude of any temperature-driven measurement bias.

While the gravimetric inter-comparison was limited to two seven-day periods, the consistency of bias magnitude and sign across contrasting thermal regimes suggests that any residual temperature-dependent effects are small relative to the observed seasonal concentration differences.

Overall, the inter-comparison strengthens confidence in the ability of the Airly sensors to capture meaningful temporal variability in particulate matter under real-world conditions. Although the gravimetric comparison is necessarily limited in duration, it provides quantitative bounds on sensor bias across contrasting thermal regimes and supports the interpretation that the long-term patterns reported in this study primarily reflect physical and atmospheric processes rather than systematic measurement error.

Fine PM and NO_2 emerge as complementary indicators of exposure. $PM_{2.5}$ exhibits strong seasonal modulation, with winter mean concentrations approximately three times higher than summer values. This pattern is consistent with reduced atmospheric dispersion during winter, characterized by shallow boundary layers, frequent thermal inversions, and lower wind speeds, which promote pollutant accumulation. Importantly, the persistence of pronounced weekday diurnal peaks throughout the year indicates that traffic activity remains the dominant emission source across all seasons, while meteorological conditions determine whether these emissions disperse or accumulate. NO_2 shows a different statistical signature: although seasonal differences are present, NO_2 exhibits stronger intra-day variability than $PM_{2.5}$, reflecting its short atmospheric lifetime and tight coupling to emission timing and proximity.

The contrasting behavior of O_3 provides further insight into the underlying chemical regime. O_3 concentrations peak during spring and summer and are suppressed during periods of intense traffic activity. The moderate negative correlations between O_3 and both $PM_{2.5}$ and NO_2 reflect classical urban photochemistry, in which freshly emitted nitric oxide (NO) rapidly titrates O_3 near roadways [38]. In this context, O_3 does not act as a driver of primary pollutant concentrations but instead serves as a diagnostic indicator of the balance between fresh emissions and photochemical processing. Elevated O_3 concentrations therefore indicate conditions of reduced local NO_x influence and enhanced regional photochemical production.

Correlation analysis further clarifies pollutant interactions. The weak inverse correlation between $PM_{2.5}$ and NO_2 suggests that, despite a shared traffic origin, their temporal variability is governed by different processes. Fine particles are subject to accumulation and multi-day persistence under stable conditions, whereas NO_2 responds rapidly to changes in traffic flow and dilution [39,40]. The stronger inverse relationships involving O_3 highlight its distinct chemical regime and reinforce its role as an indicator rather than a causal factor in PM or NO_2 variability.

Size-resolved PM measurements provide additional mechanistic insight. The close temporal alignment between PM_1 and $PM_{2.5}$ indicates dominance of combustion-related particles, which are emitted directly in the fine size range and can also form through secondary processes. These particles exhibit relatively long atmospheric residence times under stable conditions, contributing to wintertime accumulation. Seasonal and diurnal concentration patterns are consistent with known dispersion mechanisms. Reduced wind speeds and shallow boundary layers during winter favor accumulation of fine particles, while enhanced mixing in summer promotes dilution. Wind direction modulates direct exposure to traffic emissions at the stop, and precipitation contributes episodic washout effects that primarily affect short-term variability rather than systematic patterns [41]. In contrast, PM_{10} includes a substantial coarse fraction influenced by mechanical processes such as brake and tire wear, road dust resuspension, and vehicle-induced turbulence. These sources are more sensitive to surface moisture, wind speed, and traffic-induced airflow, resulting in weaker diurnal structure and greater variability compared with fine particles [42].

The heat-map analyses reinforce these interpretations by revealing systematic diurnal and seasonal structure. Weekday rush-hour peaks in $PM_{2.5}$ and NO_2 reflect emission

timing and commuter activity, while reduced weekend concentrations indicate lower traffic intensity. Amplification of these patterns during winter underscores the role of dispersion limitations, whereas their attenuation during summer reflects enhanced convective mixing. O_3 displays an opposing structure, with midday and summertime maxima and minimal weekday–weekend differentiation, consistent with its secondary formation and sensitivity to solar radiation [43].

Predictive modelling results provide an additional layer of validation. The strong performance of simple persistence models confirms that pollutant concentrations exhibit substantial short-term temporal continuity, reflecting stable emission patterns and slowly varying meteorological conditions. The improvement achieved by linear and random forest models demonstrates that meteorological variables and cyclic temporal indicators add explanatory power beyond persistence alone. For PM, the comparable performance of linear and non-linear models suggests that PM dynamics at this site are governed largely by regular, repeatable processes. In contrast, the superior performance of non-linear models for NO_2 and O_3 indicates more complex interactions involving rapid chemical reactions, threshold effects, and non-linear dispersion processes.

From an exposure perspective, the predictive models reinforce the descriptive findings by identifying periods of systematically elevated concentrations that are statistically learnable and reproducible. Weekday rush hours, particularly during winter and transitional seasons, consistently emerge as critical exposure windows. This is especially relevant for public transport stops, where individuals remain stationary within a semi-enclosed structure and are directly exposed to traffic emissions.

Finally, the influence of wind direction highlights the importance of microscale flow and site geometry. When the monitoring location is downwind of the adjacent roadway, direct transport of fresh emissions leads to elevated NO_2 and PM concentrations. Small shifts in wind direction can therefore result in substantial short-term changes in exposure, a phenomenon that is not resolved by area-wide background monitoring. The semi-enclosed configuration of the transport stop further modulates airflow and dilution, reinforcing the need for localized measurements when assessing exposure in such settings.

From a regulatory and exposure perspective, the observed concentration patterns indicate that pollutant levels at the roadside public transport stop frequently approach or exceed established air quality benchmarks during specific periods. Wintertime $PM_{2.5}$ concentrations regularly exceeded the EU annual mean limit value, reflecting sustained accumulation under reduced dispersion conditions rather than isolated episodic events. NO_2 concentrations showed short-term peaks during weekday rush hours that intermittently approached hourly guideline thresholds, highlighting the influence of direct exposure to fresh traffic emissions in close proximity to the roadway. O_3 concentrations, while generally suppressed during traffic-intensive periods due to titration, reached elevated levels during spring and summer that were comparable to target values used for health protection. These findings demonstrate that exceedances are strongly time-dependent and microenvironment-specific, reinforcing the limitation of area-wide background monitoring for assessing exposure at transport stops. The results underscore the importance of high-resolution, localized measurements for identifying critical exposure windows relevant to public health.

The study is based on a single roadside public transport stop and is therefore not intended to represent all urban environments. Instead, it provides a detailed characterization of a transport-related microenvironment, which is precisely the scale at which exposure occurs for commuters and which is often underrepresented in regulatory monitoring.

Overall, the integration of long-term monitoring, multi-pollutant analysis, and predictive modelling provides a mechanistically consistent interpretation of air quality dynamics

at a roadside public transport stop. The findings demonstrate how emission timing, atmospheric dispersion, chemical transformation, and microscale flow jointly shape exposure-relevant pollutant patterns, and they highlight the value of low-cost sensor systems for capturing these processes in real-world urban microenvironments.

While the study provides detailed insight into roadside air quality dynamics, several limitations should be acknowledged. First, the measurements were obtained using low-cost optical and electrochemical sensors, which, although suitable for capturing temporal variability and relative concentration changes, do not achieve the absolute accuracy of reference-grade instrumentation. Sensor responses may be influenced by environmental factors such as temperature and humidity, as well as potential cross-sensitivities in electrochemical gas sensors, despite internal compensation and concurrent meteorological measurements. Second, the analysis is based on observations from a single monitoring location, which limits the spatial generalizability of the results beyond similar roadside transport microenvironments. Finally, traffic intensity was characterized using average daily volumes rather than time-resolved vehicle counts, which constrains detailed attribution of short-term concentration peaks to specific traffic events. These limitations do not affect the internal consistency of the results but should be considered when extrapolating findings to other settings or comparing absolute concentrations with regulatory monitoring data.

5. Conclusions

This study demonstrates the utility of low-cost, mobile, and energy-independent air quality sensor systems for characterizing localized roadside pollution dynamics in a transport-related urban microenvironment. By combining one year of hourly measurements with descriptive statistics, correlation analysis, and predictive modelling, the analysis provides a comprehensive and mechanistically consistent assessment of air quality at a public transport stop exposed to intense traffic activity.

The results confirm that traffic emissions define the short-term temporal structure of pollution, while meteorological conditions modulate accumulation and dispersion across seasons. Fine particulate matter ($PM_{2.5}$) exhibits strong seasonal modulation, with elevated winter concentrations driven primarily by reduced atmospheric dispersion rather than changes in emission timing. In contrast, nitrogen dioxide (NO_2) shows pronounced diurnal variability closely linked to traffic activity and proximity to emissions, reflecting its short atmospheric lifetime. Ozone (O_3) displays an opposing seasonal and diurnal behavior, consistent with its secondary formation and sensitivity to photochemical conditions and titration by freshly emitted nitrogen oxides. Together, these findings highlight the complementary roles of particulate matter, NO_2, and O_3 as indicators of exposure intensity, emission timing, and chemical regime.

Predictive modelling demonstrates that the observed patterns are not merely descriptive but are statistically robust and reproducible on short time scales. The ability to forecast one-hour-ahead concentrations with moderate to high explanatory power indicates that emission timing, persistence, and meteorology jointly govern roadside air quality. This capability has practical implications for real-time exposure assessment and supports the potential development of advisory or early-warning systems for users of public transport infrastructure.

The deployment of low-cost, solar-powered, and energy-independent sensor systems proved effective for capturing microscale variability that is typically missed by regulatory monitoring networks. Such autonomous systems are particularly well suited for targeted assessment of exposure hotspots, including public transport stops, intersections, and street canyons, where permanent infrastructure and grid power may be unavailable.

Size-resolved particulate measurements further provide valuable insight into the relative contributions of combustion-related fine particles and mechanically generated coarse particles, which is increasingly relevant as non-exhaust emissions gain importance in evolving vehicle fleets.

Importantly, the results underscore that commuters waiting at roadside public transport stops may experience elevated and recurrent exposure to traffic-related pollutants, particularly during weekday rush hours and under winter dispersion conditions. The semi-enclosed design of many transport stops, while offering shelter, can reduce ventilation and promote short-term pollutant retention, thereby amplifying exposure relative to nearby open-air environments. These findings highlight the need to consider stop design, placement, and localized mitigation measures when addressing exposure in urban transport systems.

Overall, this work emphasizes the importance of integrating high-resolution measurements with statistical and predictive analysis to inform urban air quality management at the microscale. Beyond environmental monitoring, the results demonstrate how low-cost, energy-independent gas and particulate sensor systems can be used to infer emission regimes, chemical processes, and exposure-relevant patterns in real-world urban environments.

Author Contributions: Conceptualization, D.-M.M. and I.I.; methodology, D.-M.M. and I.I.; software, D.B. and V.-S.N.; validation, I.I.; formal analysis, D.B.; investigation, D.-M.M.; resources, I.I.; writing—original draft preparation, D.-M.M.; writing—review and editing, D.-M.M.; supervision, I.I. and D.B. All authors have read and agreed to the published version of the manuscript.

Funding: This research received no external funding.

Institutional Review Board Statement: Not applicable.

Data Availability Statement: Data are contained within the article as variable values and graphical representations.

Acknowledgments: The first author gratefully acknowledges PhD coordinator Ioana Ionel for her continuous guidance, scientific insight, and support throughout the PhD studies. Her expertise, constructive feedback, and encouragement were essential to the development of this research and to the author's academic training. During the preparation of this manuscript/study, the authors used Writefull v1.0.5 and ChatGPT v5.2 for the purposes of guiding the generation of the graphical abstract, improving grammar, academic style, and coherence, as well as helping to reorganize text sections for readability. The authors have reviewed and edited the output and take full responsibility for the content of this publication.

Conflicts of Interest: The authors declare no conflicts of interest.

Abbreviations

The following abbreviations are used in this manuscript:

PM	Particulate matter
PM_1	Particulate matter with aerodynamic diameter $\leq$ 1 μm
$PM_{2.5}$	Particulate matter with aerodynamic diameter $\leq$ 2.5 μm
PM_{10}	Particulate matter with aerodynamic diameter $\leq$ 10 μm
NO	Nitric oxide
NO_2	Nitrogen dioxide
NO_x	Nitrogen oxides
O_3	Ozone
EU	European Union
R^2	Coefficient of determination
RMSE	Root mean square error

SD	Standard deviation
P90	90th percentile
hPa	Hectopascal
km/h	Kilometers per hour
°C	Degrees Celsius
$\mu g/m^3$	Micrograms per cubic meter
DC	Direct current
AC	Alternating current
PV	Photovoltaic
A	Ampere
V	Volt
Ah	Ampere-hour
ppb	parts per billion
FRM	Federal Reference Method
FEM	Federal Equivalent Method

References

1. Tavares, M.S.; Rodrigues, C.T.; Silveira de Menezes, S.L.; Moreno, A.M. Health at Risk: Air Pollution and Urban Vulnerability—Perspectives in Light of the 2030 Agenda. *Green Health* **2025**, *1*, 21. [CrossRef]
2. Costagliola, M.A.; Marchitto, L.; Giuzio, R.; Casadei, S.; Rossi, T.; Lixi, S.; Faedo, D. Non-Exhaust Particulate Emissions from Road Transport Vehicles. *Energies* **2024**, *17*, 4079. [CrossRef]
3. Altay, K.; Tirgil, A.; Yanikkaya, H. Assessing the Impact of Road Infrastructure on Air Pollution: Evidence from Türkiye. *Sustainability* **2025**, *17*, 9840. [CrossRef]
4. Correa-Ochoa, M.A.; Bedoya, R.; Gómez, L.M.; Aguiar, D.; Palacio-Tobón, C.A.; Colorado, H.A. A Review on the Characterization and Measurement of the Carbonaceous Fraction of Particulate Matter. *Sustainability* **2023**, *15*, 8717. [CrossRef]
5. Sun, J.; Wang, M.; Tian, J. Particulate Matter and Volatile Organic Compounds Emissions and Their Health Impact: Spotlight on Solid Fuel Combustion. *Toxics* **2025**, *13*, 88. [CrossRef] [PubMed]
6. Ellwanger, J.H.; Ziliotto, M.; Chies, J.A.B. Lung Deposition of Particulate Matter as a Source of Metal Exposure: A Threat to Humans and Animals. *Toxics* **2025**, *13*, 788. [CrossRef] [PubMed]
7. Streinu, D.-R.; Neagoe, O.C.; Borlea, A.; Icma, I.; Derban, M.; Stoian, D. Enhancing diagnostic precision in thyroid nodule assessment: Evaluating the efficacy of a novel cell preservation technique in fine-needle aspiration cytology. *Front. Endocrinol.* **2024**, *15*, 1438063. [CrossRef]
8. Streinu, D.R.; Stoian, D.L.; Neagoe, O.C.; Derban, M.; Ciordas, P.D.; Marian, C. Inside the Matrix: Integrated Cytology and Molecular Testing of Thyroid FNAC Samples Using a Commercial Synthetic 3D Scaffold. *Int. J. Mol. Sci.* **2025**, *26*, 11100. [CrossRef]
9. Bodor, K.; Micheu, M.M.; Keresztesi, Á.; Birsan, M.-V.; Nita, I.-A.; Bodor, Z.; Petres, S.; Korodi, A.; Szép, R. Effects of PM_{10} and Weather on Respiratory and Cardiovascular Diseases in the Ciuc Basin (Romanian Carpathians). *Atmosphere* **2021**, *12*, 289. [CrossRef]
10. Songkitti, W.; Pong-A-Mas, S.; Boonsom, C.; Aroonsrisopon, T.; Wirojsakunchai, E. Evaluation of Road Dust Resuspension from Internal Combustion Engine and Electric Vehicles of the Same Model. *Atmosphere* **2025**, *16*, 1141. [CrossRef]
11. Yoo, H.; Cho, J.; Hong, S.; Kim, I. Characteristics of Suspended Road Dust According to Vehicle Driving Patterns in an Urban Area and PM_{10} Content in Silt. *Atmosphere* **2024**, *15*, 5. [CrossRef]
12. Bhattarai, K.; Lamsal, L.; Gyawali, M.; Neupane, S.; Gautam, S.P.; Bakshi, A.; Yeager, J. Impact of Nitrogen Dioxide (NO_2) Pollution on Asthma: The Case of Louisiana State (2005–2020). *Atmosphere* **2024**, *15*, 1472. [CrossRef]
13. Mainka, A.; Żak, M. Synergistic or Antagonistic Health Effects of Long- and Short-Term Exposure to Ambient NO_2 and $PM_{2.5}$: A Review. *Int. J. Environ. Res. Public Health* **2022**, *19*, 14079. [CrossRef]
14. Lei, Q.; Li, X.; Guo, X.; Chen, J.; Yi, C. Neuropsychological Effects of Air Pollution on Children and Adolescents (0–18 Years): A Global Bibliometric Analysis. *Atmosphere* **2025**, *16*, 1164. [CrossRef]
15. Rus, A.-A.; Pescariu, S.-A.; Zus, A.-S.; Gaiță, D.; Mornoș, C. Impact of Short-Term Exposure to Nitrogen Dioxide (NO_2) and Ozone (O_3) on Hospital Admissions for Non-ST-Segment Elevation Acute Coronary Syndrome. *Toxics* **2024**, *12*, 123. [CrossRef]
16. Amialchuk, A.; Sapci, O. The Effect of Long-Term Exposure to O_3 and $PM_{2.5}$ on Allergies and Asthma in Adolescents and Young Adults. *Int. J. Environ. Res. Public Health* **2025**, *22*, 1262. [CrossRef]

17. Blaszczak-Boxe, C.; Karle, N.N.; Ideki, O.; Taku, L.; Yu, M.; Wang, S.; Golosov, N.; Riyad, M.; Hilaire, D.S.; Smith, K.; et al. Temporal variations in NO_x, O_3, and CO_2 and meteorological influences in New York and New Jersey urban atmospheres. *Discov. Environ.* **2025**, *3*, 98. [CrossRef]
18. Wang, J.; Wu, J.; Liu, B.; Liu, X.; Gao, H.; Zhang, Y.; Feng, Y.; Han, S.; Gong, X. Exploring the Sensitivity of Visibility to $PM_{2.5}$ Mass Concentration and Relative Humidity for Different Aerosol Types. *Atmosphere* **2022**, *13*, 471. [CrossRef]
19. Marinou, E.; Voudouri, K.A.; Tsikoudi, I.; Drakaki, E.; Tsekeri, A.; Rosoldi, M.; Ene, D.; Baars, H.; O'Connor, E.; Amiridis, V.; et al. Geometrical and Microphysical Properties of Clouds Formed in the Presence of Dust above the Eastern Mediterranean. *Remote Sens.* **2021**, *13*, 5001. [CrossRef]
20. Matei, E.; Râpă, M.; Mateș, I.M.; Popescu, A.-F.; Bădiceanu, A.; Balint, A.I.; Covaliu-Mierlă, C.I. Heavy Metals in Particulate Matter—Trends and Impacts on Environment. *Molecules* **2025**, *30*, 1455. [CrossRef] [PubMed]
21. Kameni Nematchoua, M. Strategies for Studying Acidification and Eutrophication Potentials, a Case Study of 150 Countries. *J* **2022**, *5*, 150–165. [CrossRef]
22. Felzer, B.S.; Cronin, T.; Reilly, J.M.; Melillo, J.M.; Wang, X. Impacts of ozone on trees and crops. *Comptes Rendus Geosci.* **2007**, *339*, 784–798. [CrossRef]
23. Emberson, L. Effects of ozone on agriculture, forests and grasslands. *Philos. Trans. A Math. Phys. Eng. Sci.* **2020**, *378*, 20190327. [CrossRef]
24. Dominici, F.; Peng, R.D.; Barr, C.D.; Bell, M.L. Protecting human health from air pollution: Shifting from a single-pollutant to a multipollutant approach. *Epidemiology* **2010**, *21*, 187–194. [CrossRef]
25. Petrić, V.; Račić, N.; Hrga, I.; Grgec, D.; Marić, M.; Krivohlavek, A.; Anić, Z.; Lovrić, M.; Jergović, M. Assessment of Sensor Data from an Air Quality Monitoring Network—The Need for Machine Learning-Based Recalibration and Its Relevance in Health Impact Analysis of Local Pollution Events. *Atmosphere* **2025**, *16*, 1358. [CrossRef]
26. Shabbir, M.; Saeed, T.; Saleem, A.; Bhave, P.; Bergin, M.; Khokhar, M.F. A paradigm shift: Low-cost sensors for effective air quality monitoring and management in developing countries. *Environ. Int.* **2025**, *200*, 109521. [CrossRef]
27. De Vito, S.; Del Giudice, A.; D'Elia, G.; Esposito, E.; Fattoruso, G.; Ferlito, S.; Formisano, F.; Loffredo, G.; Massera, E.; D'Auria, P.; et al. Future Low-Cost Urban Air Quality Monitoring Networks: Insights from the EU's AirHeritage Project. *Atmosphere* **2024**, *15*, 1351. [CrossRef]
28. Jeong, C.-H.; Fang, C.; Evans, G. Spatial variation of resuspended particulate matter in urban environments and real-world assessment of street sweeping. *Environ. Pollut.* **2025**, *373*, 126165. [CrossRef]
29. Airly. Available online: https://airly.org/en/solutions/measure/ (accessed on 28 December 2025).
30. Chicea, D.; Leca, C.; Olaru, S.; Chicea, L.M. An Advanced Sensor for Particles in Gases Using Dynamic Light Scattering in Air as Solvent. *Sensors* **2021**, *21*, 5115. [CrossRef]
31. Khan, T.R.; Emerson, Z.I.; Mentz, K.H. Evaluation of Fine Particulate Matter ($PM_{2.5}$) Concentrations Measured by Collocated Federal Reference Method and Federal Equivalent Method Monitors in the U.S. *Atmosphere* **2024**, *15*, 978. [CrossRef]
32. Laref, R.; Losson, E.; Sava, A.; Siadat, M. Field Nitrogen Dioxide and Ozone Monitoring Using Electrochemical Sensors with Partial Least Squares Regression. *Chem. Proc.* **2021**, *5*, 61. [CrossRef]
33. Schmitz, S.; Caseiro, A.; von Schneidemesser, E. How electrochemical sensors measure up to reference-grade nitrogen dioxide monitors across temporal scales. *Sci. Total Environ.* **2025**, *980*, 179476. [CrossRef]
34. Airly. How Do Air Pollution Sensors Work? Our Experts Explain. Available online: https://airly.org/en/how-do-air-pollution-sensors-work-our-experts-explain/ (accessed on 28 December 2025).
35. *ISO/IEC 17025:2017*; General Requirements for the Competence of Testing and Calibration Laboratories. ISO: Geneva, Switzerland, 2017. Available online: https://www.iso.org/standard/66912.html (accessed on 18 January 2026).
36. EUR-Lex. Directive 2008/50/EC of the European Parliament and of the Council of 21 May 2008 on ambient air quality and cleaner air for Europe. *Off. J. Eur. Union* **2008**, *L 152*, 1–44.
37. Romanian Law no. 104 from 15 June 2011 in Relation to Air Quality (Original in Romanian: LEGE nr. 104 Din 15 Iunie 2011 Priving Calitatea Aerului Înconjurător) Parliament of Romania. Available online: https://legislatie.just.ro/Public/DetaliiDocument/129642 (accessed on 28 December 2025).
38. Chatoutsidou, S.E.; Kordonouri, I.; Lazaridis, M. An Air-Quality-Based Analysis of NO, NO_2, and O_3 at a Suburban Mediterranean Site. *Atmosphere* **2026**, *17*, 7. [CrossRef]
39. Jiang, Q.; Zhang, H.; Wang, F.; Wang, F. Research on the Growth Mechanism of $PM_{2.5}$ in Central and Eastern China during Autumn and Winter from 2013–2020. *Atmosphere* **2022**, *13*, 134. [CrossRef]
40. Curier, R.L.; Kranenburg, R.; Segers, A.J.S.; Timmermans, R.M.A.; Schaap, M. Synergistic use of OMI NO_2 tropospheric columns and LOTOS–EUROS to evaluate the NO_x emission trends across Europe. *Remote Sens. Environ.* **2014**, *149*, 58–69. [CrossRef]
41. Kumar, C.P.; Akhilesh, K.; Vineet, P.; Kumar, S.A. Seasonal characteristics of PM_1, $PM_{2.5}$, and PM_{10} over Varanasi during 2019–2020. *Front. Sustain. Cities* **2022**, *4*, 909351. [CrossRef]

42. Yoo, H.; Yeon, G.; Kim, I. Theoretical Analysis of Suspended Road Dust in Relation to Concrete Pavement Texture Characteristics. *Atmosphere* **2025**, *16*, 761. [CrossRef]
43. Fang, C.; Wang, L.; Wang, J. Analysis of the Spatial–Temporal Variation of the Surface Ozone Concentration and Its Associated Meteorological Factors in Changchun. *Environments* **2019**, *6*, 46. [CrossRef]

Disclaimer/Publisher's Note: The statements, opinions and data contained in all publications are solely those of the individual author(s) and contributor(s) and not of MDPI and/or the editor(s). MDPI and/or the editor(s) disclaim responsibility for any injury to people or property resulting from any ideas, methods, instructions or products referred to in the content.